Scientific Research Publishing

Materials Sciences and Applications, 2017, 8, 838-847
http://www.scirp.org/journal/msa
ISSN Online: 2153-1188
ISSN Print: 2153-117X

Formation of Germanium-Carbon Core-Shell Nanowires by Laser Vaporization in High-Pressure Ar Gas without the Addition of Other Metal Catalysts

Kazuya Hatano, Yuuki Asano, Yuuto Kameda, Akira Koshio, Fumio Kokai*

Division of Chemistry for Materials, Graduate School of Engineering, Mie University, Tsu, Japan
Email: *kokai@chem.mie-u.ac.jp

How to cite this paper: Hatano, K., Asano, Y., Kameda, Y., Koshio, A. and Kokai, F. (2017) Formation of Germanium-Carbon Core-Shell Nanowires by Laser Vaporization in High-Pressure Ar Gas without the Addition of Other Metal Catalysts. *Materials Sciences and Applications*, **8**, 838-847.
https://doi.org/10.4236/msa.2017.812061

Received: September 12, 2017
Accepted: November 4, 2017
Published: November 7, 2017

Abstract

Germanium (Ge)-carbon (C) core-shell nanowires (NWs), 15 - 80 nm thick and <1 μm long, were grown using continuous-wave laser vaporization of Ge-graphite composite targets in high pressure (0.1 - 0.9 MPa) Ar gas. The NW core was crystalline Ge and the shell was amorphous C. The fraction of the NWs in deposits was changed significantly by the Ge content in the targets and had a maximum at the Ge content of 40 atomic %. With increasing Ar pressure, thicker NWs were grown. A strong correlation was evident between the two diameters of the NW and nanoparticle (NP) attached with the tip of the NW. The growth of the NWs can be explained by the formation of Ge-C liquid-like molten NPs having a specific range of size and composition and precipitation of Ge and C followed by phase separation.

Keywords

Laser Vaporization, Germanium, Carbon, Nanowire, Core Shell

1. Introduction

One-dimensional semiconductor nanowires (NWs) have attracted much interest due to their size effects and novel properties. Among various NWs, silicon (Si) NWs have been preferentially studied since Si is of great technological importance in a wide range of applications such as electronic and optoelectronic devices and chemical biological sensors. Germanium (Ge) NWs have also been studied since Ge provides properties that are superior to those of Si in device applications such as a higher carrier mobility and a larger Bohr exciton radius [1].

However, Ge NWs were easily oxidized upon exposure to oxygen and water and their oxide layers reached a thickness of ~4 nm for ~24 h [2]. Since the oxide exhibited poor chemical stability [3], some methods including coating by organic monolayers [4] and encapsulation by carbon (C) [5] [6] [7] were studied to prevent the oxidation of Ge NWs.

More recently, Ge NWs have also gained attention in the research and development of lithium-ion secondary batteries having an alternative anode material of graphite [8]. The use of metallic anode materials such as Ge, Si, and tin that undergo lithium alloying reactions provides higher capacities than that of graphite. However, large volume changes occur in the metallic anode materials during lithium alloying/de-alloying processes, resulting in their pulverization. Using nanostructured materials like Ge NWs is expected to be a promising strategy to overcome the large volume change and to preserve the structural integrity. Ge NWs coated with C have also been studied [9] [10] as well as Ge NWs, because C plays an important role in forming conductive networks in addition to preventing oxidation.

We have succeeded in forming some one-dimensional nanostructures, such as carbon nanotubes (CNTs) filled with Cu [11] or SiC [12] and amorphous silicon oxide (SiO_x) NWs [13] using continuous wave (CW) laser vaporization in high-pressure (0.1 - 0.9 MPa) Ar gas without the addition of other metal catalysts. Our laser vaporization is a simple method, and it can grow composite one-dimensional nanostructures through a strong interaction of vaporized species with low expansion velocities (10^2 - 10^3 cm/s) [14] in a confined space by high-pressure Ar gas. In this paper, we report on our successful synthesis of Ge-C core-shell composite NWs, and we discuss the growth mechanism of the NWs. Composite NWs with Ge crystalline cores can be grown in a single step. Although the degree of encapsulation of Ge NWs by C is not clear in some studies [6] [9] [12], the formation of Ge NWs completely encapsulated with C is strongly desired like Ge NWs in multi-walled CNTs [7]. Unlike the syntheses of Ge-C NWs using arc discharge [15] or pyrolysis [5], our composite NWs are completely filled with Ge and hollow C structures are not presented, although NPs are formed as by-products.

2. Experimental Part

Laser vaporization of Ge-graphite composite (Ge content: 5 - 100 atomic (at.) %) targets was carried out in the presence of Ar gas as reported in previous studies [11] [12] [13]. Ge powder (Aldrich, 99.99% purity and 0.5 - 147 μm grain size) was mixed with graphite powder (Toyo Tanso, 99.9% purity and ~4 μm grain size). The mixed powder was pressed in to Ge-graphite cylindrical targets (14-mm diameter and 10-mm height) and installed in a stainless-steel chamber. Prior to filling the chamber with Ar gas, it was evacuated to ~10^{-1} Pa using a rotary pump and flushed three times with Ar gas. Then, it was filled with Ar gas at pressures ranging from 0.1 to 0.9 MPa. A CW Nd: YAG laser (Lee Laser, Series

800, 1.06 μm wavelength, and 500 W peak power) was used for the vaporization of Ge-graphite targets at room temperature. The laser beam was focused on the target through a quartz window. The laser spot size and power density on the target were adjusted to 2 mm and about 18 kW/cm^2, respectively, and the laser irradiation time was set to 2 s.

After laser vaporization using a single laser shot, the deposits in the chamber were collected and examined with a scanning electron microscope (SEM, Hitachi, S-4800) and a transmission electron microscope (TEM) operating at 100 kV (Hitachi, H-7000). Raman spectra of the deposits were taken using a Raman spectrometer (Jobin Yvon, T-640000M1) with excitation by means of the 488-nm line of an Ar^+ laser. Deposits obtained after 20 laser shots were collected and used to measure the powder x-ray diffraction (XRD) patterns on an x-ray diffractometer (Rigaku, Ultima IV) or the x-ray photoelectron (XPS) spectra on a spectrometer (Shimadu, ESCA-3400) using a MgKα x-ray source. The peak position of the main component in the C 1s core level spectrum was assumed to be 284.6 eV for calculating the binding energies of each peak.

3. Results and Discussion

Depending on the Ge content, deposits of different morphologies were obtained. **Figure 1** shows typical SEM images of deposits obtained at Ge contents of 5, 10, 40, 60, 80, and 100 at.%. A constant Ar gas pressure of 0.1 MPa was used. As seen in **Figure 1(a)**, particles were main products at a low Ge content. Graphitic polyhedra with diameters of 150 - 500 nm as observed in previous studies [16] [17] were dominant at a Ge content of 5 at.%. As seen in **Figure 1(b)** and **Figure 1(c)**, when the Ge content was increased, the deposits became to contain many NWs and the fraction of NWs was maximized (~80% in deposits) at a Ge content of ~40 at.%, while NPs were presents as by-products. A further increase in the Ge content resulted in a decrease in the NW fraction and an increase in the NP fraction (**Figure 1(d)** and **Figure 1(e)**). Only Ge NPs with diameters of 30 - 590 nm were formed at a Ge content of 100 at.% (**Figure 1(f)**).

Figure 2(a) is a typical TEM image of deposits obtained at a Ge content of 40 at.%. NWs with diameters of 8 - 35 nm are seen together with NPs with diameters of 17 - 100 nm. Tips of NWs attached with NPs are seen in **Figure 2(b)** of a higher magnification TEM image of the deposits. This image also indicates that both the NWs and NPs consist of core and shell parts. Core NWs with diameters of 6 - 14 nm and shells with thicknesses of 2 - 3 nm are observed. In a selected area electron diffraction (SAED) pattern shown in the inset of **Figure 2(b)**, reflections assigned to Ge (111), (220), and (311) planes (according to JCPDS 4-545) are observed, indicating the presence of crystalline Ge. The lengths of the NWs were up to ~1 μm from the observed SEM and TEM images.

For deposits obtained at a Ge content of 40 at.%, XRD, XPS, and Raman spectrum measurements were performed. **Figure 3** shows an XRD pattern of the deposits. Sharp diffraction lines were observed and indexed to (111), (220),

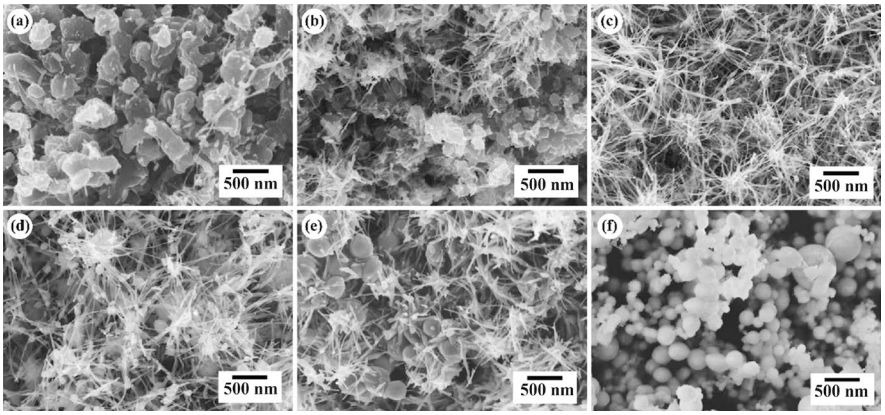

Figure 1. SEM images of deposits obtained at Ge content of (a) 5; (b) 10; (c) 40; (d) 60; (e) 80; and (f) 100 at.% and Ar pressure of 0.1 MPa.

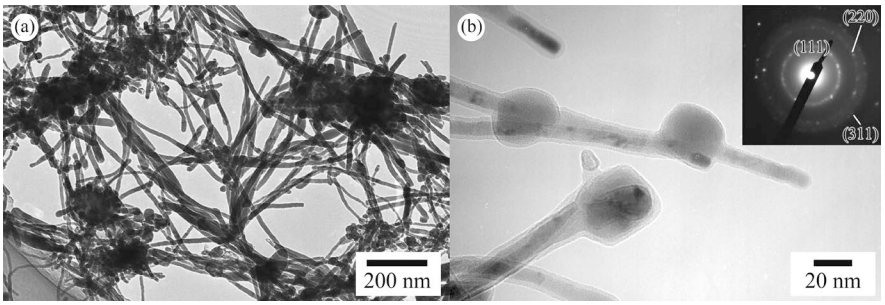

Figure 2. (a) Typical TEM image of deposits obtained at Ge content of 40 at.% and Ar pressure of 0.1 MPa and (b) TEM image of NWs and their tip parts in deposits, and inset: corresponding SAED pattern.

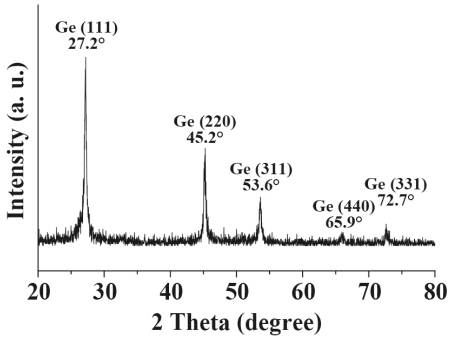

Figure 3. XRD pattern of deposits obtained at Ge content of 40 at.% and Ar pressure of 0.1 MPa.

(311), (440), and (331) reflections of a face-centered cubic Ge crystal. Ge, C, and O atoms were detected from XPS measurements. Their peak positions in the XPS spectrum were very close to those already reported in the literature [18] [19] [20]. **Figure 4** shows Ge 3d and C 1s XPS spectra of deposits. To investigate the type of chemical bonds in the deposits, we deconvoluted the Ge 3d and C 1s spectra into components using references to previous studies [18] [19] [20]. In the Ge 3d spectrum, the main component with a peak at 29.4 eV was assigned to Ge atoms bonded to Ge. The other two components at 30.1 and 32.5 eV were as

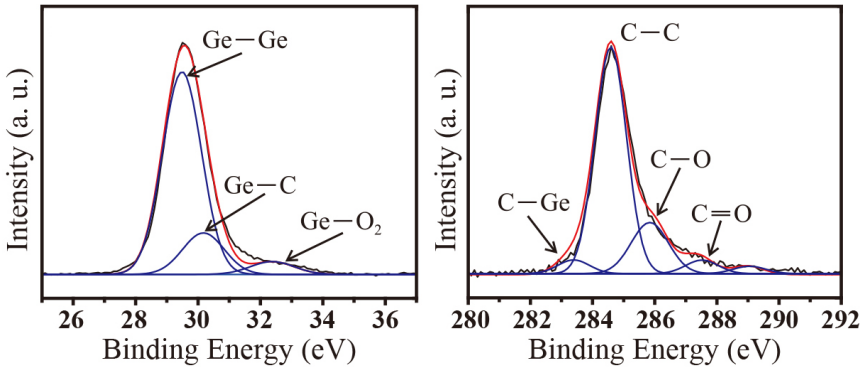

Figure 4. (a) Ge 3d and (b) C 1s XPS spectra of deposits obtained at Ge content of 40 at.% and Ar pressure of 0.1 MPa.

signed to Ge atoms bonded to C and to oxidized Ge atoms, respectively. The presence of the major metallic Ge-Ge component was consistent with the SAED and XRD patterns. The low-intensity Ge-O_2 component indicates that the C layer is effective to prevent the oxidation of the Ge NWs. In the C 1s spectrum, a major component at 284.6 eV was assigned to C atoms bonded to C. At lower energy, a minor component at 283.3 eV was assigned to C atoms bonded to Ge. At higher energy, two other components at 285.9 and 287.7 eV were assigned to C atoms bonded to O. The atomic ratio of O/Ge was estimated to be approximately 0.18 from the XPS spectra. The O atoms bonded to the Ge and C atoms were suggested to be 37% and 63%, respectively. **Figure 5** shows the Raman spectra of deposits at two frequency regions. In the low frequency region, a sharp band was observed at 296 cm^{-1} and assigned to a Ge-Ge stretching mode (optical phonon) [21] [22]. This band exhibited a tailing towards a lower frequency, indicating the probable presence of amorphous Ge materials [21] such as Ge NPs as by-products. In the high frequency region, broad D (related to defect density) and G (related to E_{2g} vibrational mode of graphite lattice) bands with full widths at half maximum of 173 and 113 cm^{-1}, respectively, were observed at 1352 and 1586 cm^{-1}, indicating the presence of amorphous C. From these findings in XRD, XPS, and Raman spectroscopy, and from the contrast in the TEM image (**Figure 2(b)**), the core and shell of the grown NW were identified to be crystalline Ge and amorphous C, respectively. No clear graphene layer indicating the formation of a multi-walled CNT was evident from the TEM observation of the shell part. Ge NWs were reported to be highly sensitive to oxidation upon exposure to oxygen and water [2]. The low intensity oxidized Ge component at 32.5 eV in the Ge 3d XPS spectrum (**Figure 4(a)**) indicates that the amorphous C shells act to depress the oxidation of Ge cores.

Thicker NWs were obtained under higher Ar gas pressure conditions. **Figure 6** shows examples of SEM and TEM images of deposits obtained at Ar pressures of 0.5 and 0.9 MPa. The Ge content in the targets was 40 at.%. Thicker NWs with diameters of 20 - 60 and 20 - 80 nm were grown at 0.5 and 0.9 MPa, respectively. In the higher magnification TEM images (**Figure 6(c)** and **Figure 6(d)**),

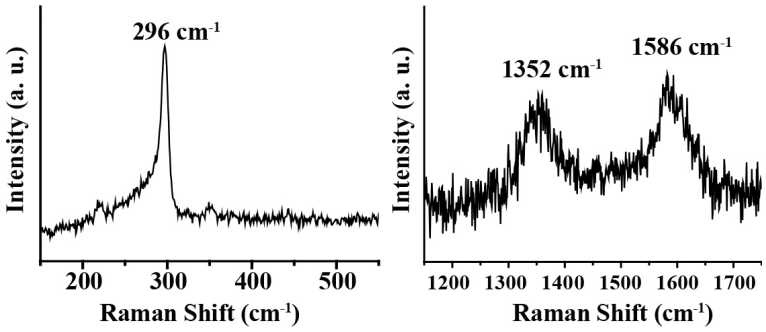

(a) (b)

Figure 5. Raman spectra observed at two regions of (a) 150 - 550 and (b) 1150 - 1750 cm^{-1} of deposits obtained at Ge content of 40 at.% and Ar pressure of 0.1 MPa.

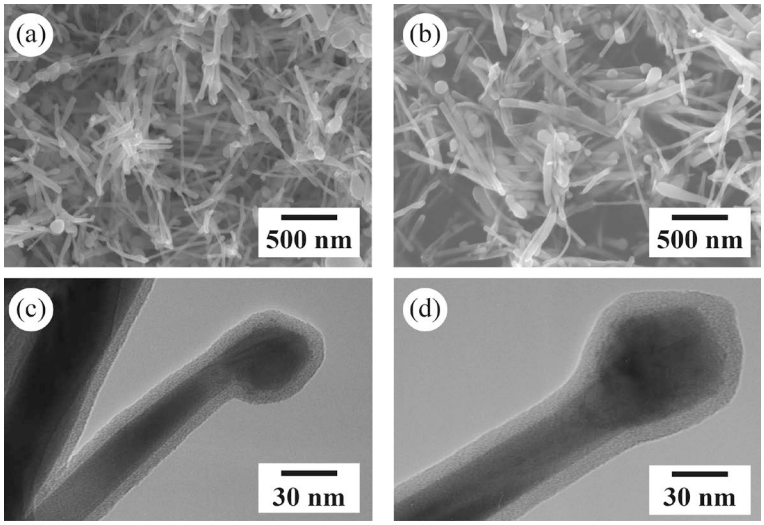

Figure 6. SEM and TEM images of deposits obtained at Ar pressures of (a) (c) 0.5 and (b) (d) 0.9 MPa.

core-shell NWs attached with NPs were observed, similar to those in **Figure 2(b)**. We checked more than 400 NWs; no hollow structure like a multi-walled CNT was observed, and Ge cores were present from the roots to the tips.

Each of the diameters of NWs and NPs attached with tips of the NWs were measured for more than 400 samples obtained at 0.1, 0.5, and 0.9 MPa. **Figure 7** shows plots of the tip NP diameter versus the NW diameter. The larger diameter values of the NWs were plotted for the NWs grown at higher Ar pressures corresponding to the observation in the SEM and TEM images (**Figure 6**). A strong correlations between the NP and NW diameters were evident, similar to the ones in our previous study of SiO_x NW growth using Si and Si/SiO_2 targets [13]. The correlation coefficients were calculated to be 0.80, 0.78, and 0.81 for the samples obtained at 0.1, 0.5, and 0.9 MPa, respectively.

Because of the presence of NPs attached with NWs and the strong correlations of the diameters with those of NWs, we believe that liquid-like molten NPs act as seeds for the growth of NWs at high temperature. Ge-filled CNTs have been

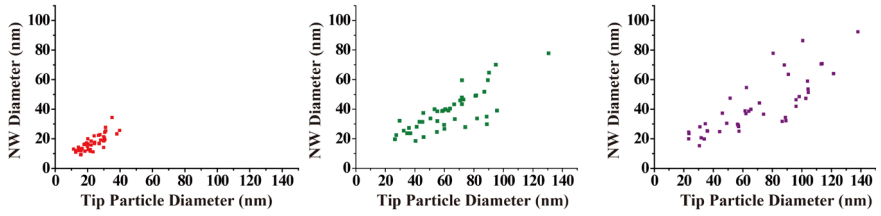

Figure 7. Plots of NW diameter versus tip NP diameter obtained at (a) 0.1; (b) 0.5; and (c) 0.9 MPa.

formed by arc discharge [15]. However, some of the CNTs produced were intermittently filled and unfilled CNTs were unavoidably produced. A general mechanism proposed for the formation of the metal-filled CNTs was precipitation of C and simultaneous metal filling into the precipitated hollow tubes [7] [11] [23]. Because our Ge-C core-shell NWs were completely filled with Ge, we do not think the precipitation and filling mechanism operates for the growth of our Ge-C NWs. Instead, we propose a growth mechanism, similar to that of amorphous SiO_x NWs from supersaturated Si-rich molten SiO_x NPs in a vapor-liquid-solid process [13] based on a binary Si-O phase diagram, which has a region of coexistence of liquid Si and O and solid SiO_x. We believe that precipitation of Ge and C simultaneously occurs from supersaturated molten Ge-C particles along with a temperature drop. An important finding in our experiment was the presence of a suitable target composition (~40 at.% of Ge) for the Ge-C core-shell NW growth. Molten Ge-C NPs having a specific range of size and composition are thought to act as seeds to nucleate and grow the NWs. The TEM images of **Figure 2(b)**, **Figure 6(c)**, and **Figure 6(d)** indicate that the volume of Ge relative to C in tip NPs is larger than that in NWs grown from the corresponding tip NPs, although the NPs and NWs are final solid products after the drop in temperature. Similar to the growth of the SiO_x NWs, Ge-rich molten NPs may act to grow the NWs, where Ge has both a catalyst-like behavior and a role as a precipitation material together with C. Unfortunately, a detailed binary Ge-C phase diagram is not available in the literature [24]. The formation of molten Ge-C NPs may be a phenomenon peculiar to nano-sized particles, because of an extremely low solubility of C in bulk Ge, which was too low to measure [25]. An enhanced collisional interaction of Ge and C species such as clusters occurring in a space confined by Ar gas may lead to the formation of composite molten NPs at high temperature. After the precipitation of Ge and C from the molten NPs, a phase separation between Ge and C may result in the final structures of the Ge-C core-shell NWs. A catalytic behavior of Ge for C in nano-sized particles was reported for the growth of single and double walled CNTs [26]. However, the yield of the CNTs was very much low, compared to those using metals such as iron, cobalt, and nickel. As seen in **Figure 1(c)**, the growth of our core-shell NWs was fairy efficient.

Successive anisotropic precipitation of Ge and C from the molten Ge-C NP is

required for the NW growth. A higher level in the supersaturation of Si, compared to that for the stage of successive Si NW growth, was reported for the nucleation of Si NWs from Au-Si molten NPs [27]. As seen in the TEM images of **Figure 2**, the anisotropic precipitation continued in almost all NWs. In other words, more than two NWs did not grow from a single molten NP. We believe that after the nucleation of the Ge-C core-shell NWs, phenomena resulting in higher level supersaturation such as a change in the supply of Ge and C species to the molten NPs and a rapid temperature drop are not likely to occur in Ar gas after laser vaporization.

4. Conclusion

A simple method of forming Ge-C core-shell NWs was presented by means of CW laser irradiation onto Ge-graphite targets in the presence of high-pressure Ar gas. SEM and TEM examinations indicated that deposits with different morphologies such as graphitic polyhedra, Ge NPs, and core-shell NWs were formed depending on the Ge content in the targets. The fraction of the NWs in the deposits maximized at a Ge content of ~40 at.%. The higher magnification TEM image, SAED pattern, XRD pattern, XPS spectra, and Raman spectra of the deposits indicated that the NWs consisted of crystalline Ge cores and amorphous C shells. The low-intensity Ge-O_2 component in the XPS spectrum indicates that the C layer is effective to prevent the oxidation of the Ge NWs. As the Ar gas pressure increased, thicker Ge-C core-shell NWs were obtained. The growth of the NWs was explained by the formation of liquid-like molten Ge-C NPs having a specific range of size and composition acting as seeds to nucleate and grow the NWs in a space confined by Ar gas. Further work is needed to clarify the nucleation and growth processes of the NWs and the conductive properties of the C shells.

Acknowledgements

The authors are grateful for the "Kakenhi (15K04606)" Grant-in-Aid for Scientific Research provided by the Japan Society for the Promotion of Science in support of this work.

References

[1] O'Regon, C., Biswas, S., Petkov, N. and Holmes, J.D. (2014) Recent Advances in the Growth of Germanium Nanowires: Synthesis, Growth Dynamics and Morphology Control. *Journal of Materials Chemistry C,* **2**, 14-33. https://doi.org/10.1039/C3TC31736F

[2] Hanrath, T. and Korgel, B.A. (2004) Chemical Surface Passivation of Ge Nanowires. *Journal of American Chemical Society,* **126**, 15466-15472. https://doi.org/10.1021/ja0465808

[3] Tabet, N., Al-Sadah, J. and Salim, M. (1999) Growth of Oxide Layer Germanium (011) Substrate under Dry and Wet Atmospheres. *Surface Review and Letters,* **6**, 1053-1063. https://doi.org/10.1142/S0218625X99001141

[4] Wang, D., Chang, Y.-L., Liu, Z. and Dai, H. (2005) Oxidation Resistant Germanium Nanowires: Bulk Synthesis, Long Chain Alkanethiol Functionalization, and Langmuir-Blodgett assembly. *Journal of American Chemical Society,* **127**, 11871-11875. https://doi.org/10.1021/ja053836g

[5] Wu, Y. and Yang, P. (2000) Germanium/Carbon Core-Sheath Nanostructures. *Applied Physics Letters*, **77**, 43-45. https://doi.org/10.1063/1.126871

[6] Sutter, E. and Sutter, P. (2006) Au-Induced Encapsulation of Ge Nanowires in Protective C Shells. *Advanced Materials*, **18**, 2583-2588. https://doi.org/10.1002/adma.200600624

[7] Pandurangan, A., Morin, C., Qian, D., Andrews, R. and Crocker, M. (2009) Single-Step Synthesis of Germanium Nanowires Encapsulated within Multi-Walled Carbon Nanotubes. *Carbon*, **47**, 1708-1714. https://doi.org/10.1016/j.carbon.2009.02.019

[8] Ji, L., Lin, Z., Alcoutlabi, M. and Zhang, X. (2011) Recent Developments in Nanostructured Anode Materials for Rechargeable Lithium-Ion Batteries. *Energy & Environmental Science*, **4**, 2682-2699. https://doi.org/10.1039/c0ee00699h

[9] Seo, M., Park, M., Lee, K.T., Kim, K., Kim, J. and Cho, J. (2011) High performance Ge Nanowire Anode Sheathed with Carbon for Lithium Rechargeable Batteries. *Energy & Environmental Science*, **4**, 425-428. https://doi.org/10.1039/C0EE00552E

[10] Liu, J., Song, K., Zhu, C., Chen, C., van Aken, P.A., Maier, J. and Yu, Y. (2014) Ge/C Nanowires as High-Capacity and Long-Life Anode Materials for Li-Ion Batteries. *ACS Nano*, **8**, 7051-7059. https://doi.org/10.1021/nn501945f

[11] Kokai, F., Shimazu, T., Adachi, K., Koshio, A. and Takahashi, Y. (2009) Fabrication of Completely Filled Carbon Nanotubes with Copper Nanowires in a Confined Space. *Applied Physics A*, **97**, 55-62. https://doi.org/10.1007/s00339-009-5339-3

[12] Kokai, F., Uchiyama, K., Shimazu, T. and Koshio, A. (2010) Fabrication of Two Types of One-Dimensional Si-C Nanostructures by Laser Ablation. *Applied Physics A*, **101**, 497-502. https://doi.org/10.1007/s00339-010-5886-7

[13] Kobayashi, K., Kokai, F., Sakurai, N. and Yasuda, H. (2013) Silicon-Catalyzed Growth of Amorphous SiO_x Nanowires by Laser Vaporization of Si and Si/SiO_2. *Journal of Physical Chemistry C*, **117**, 25169-25174. https://doi.org/10.1021/jp409039x

[14] Kokai, F., Takahashi, K., Yudasaka, M. and Iijima, S. (1999) Emission Spectroscopic and Shadowgraphic Studies on the Growth Dynamics of Graphitic Carbon Particles Synthesized by CO_2 Laser Vaporization. *Journal of Physical Chemistry B*, **103**, 8686-8693. https://doi.org/10.1021/jp991551i

[15] Dai, J.Y., Lauerhaas, J.M., Setlur, A.A. and Chang, R.P.H. (1996) Synthesis of Carbon-Encapsulated Nanowires Using Polycyclic Aromatic Hydrocarbon Precursors. *Chemical Physics Letters*, **258**, 547-553. https://doi.org/10.1016/0009-2614(96)00709-9

[16] Kokai, F., Takahashi, K., Kasuya, D., Nakayama, A., Koga, Y., Yudasaka, M. and Iijima, S. (2003) Laser Vaporization Synthesis of Polyhedral Graphite. *Applied Physics A*, **77**, 69-71. https://doi.org/10.1007/s00339-003-2128-2

[17] Kokai, F., Takakuwa, N., Koshio, A. and Takahashi, K. (2006) Effect of Silicon on the Formation of Graphitic Polyhedral and Balloon-Like Particles. *Applied Physics A*, **84**, 391-394. https://doi.org/10.1007/s00339-006-3638-5

[18] Briggs, D. and Seah, M.P. (1983) Practical Surface Analysis by Auger and X-Ray Photoelectron Spectroscopy. John Wiley & Sons, Chichester, 499 p.

[19] Vilcarromero, J. and Marques, F.C. (2000) XPS Study of the Chemical Bonding in Hydrogenated Amorphous Germanium-Carbon Alloys. *Applied Physics A*, **70**, 581-585. https://doi.org/10.1007/s003390051083

[20] Nguyen, P., Ng, H.T. and Meyyappan, M. (2005) Growth of Individual Vertical Germanium Nanowires. *Advanced Materials*, **17**, 549-553. https://doi.org/10.1002/adma.200400908

[21] Mathur, S., Shen, H., Sivakov, V. and Werner, U. (2004) Germanium Nanowires and Core-Shell Nanostructures by Chemical Vapor Deposition of $Ge(C_5H_5)_2$. *Chemistry of Materials*, **16**, 2449-2456. https://doi.org/10.1021/cm031175l

[22] Pei, L.Z., Zhao, H.S., Tan, W., Yu, Y., Chen, Y.W., Fan, C.G. and Zhang, Q.-F. (2009) Smooth Germanium Nanowires Prepared by a Hydrothermal Deposition Process. *Materials Characterization*, **60**, 1400-1405. https://doi.org/10.1016/j.matchar.2009.05.003

[23] Demoncy, N., Stéphen, O., Brun, N., Colliex, C., Loiseau, A. and Pascard, H. (1998) Filling Carbon Nanotubes with Metals by the Arc-Discharge Method: The Key Role of Sulfur. *The European Physical Journal B*, **4**, 147-157. https://doi.org/10.1007/s100510050363

[24] Massalski, T.B., Okamoto, H., Subramanian, P.R. and Kacprzak, L. (1990) Binary Alloy Phase Diagrams. Vol. 1, The Materials Information Society, ASM International, 849 p.

[25] Scace, R.I. and Slack, G.A. (1959) Solubility of Carbon in Silicon and Germanium. *Journal of Chemical Physics*, **30**, 1551-1555. https://doi.org/10.1063/1.1730236

[26] Takagi, D., Hibino, H., Suzuki, S., Kobayashi, Y. and Homma, Y. (2007) Carbon Nanotube Growth from Semiconductor Nanoparticles. *Nano Letters*, **7**, 2272-2275. https://doi.org/10.1021/nl0708011

[27] Kim, B.J., Tersoff, J., Kodambaka, S., Reuter, M.C., Stach, E.A. and Ross, F.M. (2008) Kinetics of Individual Nucleation Events Observed in Nanoscale Vapor-Liquid-Solid Growth. *Science*, **322**, 1070-1073. https://doi.org/10.1126/science.1163494